Nanospheres of Silica with an ε-Fe_2O_3 Single Crystal Nucleus

Elena Taboada,[†] Martí Gich,[‡] and Anna Roig[†,*]

[†]Institut de Ciència de Materials de Barcelona (ICMAB-CSIC), Campus de la UAB, 08193 Bellaterra, Spain, and [‡]Saint-Gobain Recherche, 93303 Aubervilliers, France

ABSTRACT A route to produce single crystals of ε-Fe_2O_3 individually wrapped in a silica shell is presented. Formation of ε-Fe_2O_3/silica nanospheres was achieved by controlled recrystallization of maghemite particles confined in silica shells *via* calcination in air. Phase transition was monitored by X-ray diffraction, magnetometry, and transmission electron microscopy. Core−shell nanocomposite particles can be dispersed as a colloidal suspension in several polar liquids enlarging the processability spectrum of the material and thus facilitating the use of ε-Fe_2O_3 in technological applications and its integration in devices.

KEYWORDS: magnetic nanoparticles · iron oxide · ε-Fe_2O_3 · core−shell · phase transitions · silica nanocomposite

Epsilon iron−oxide is a metastable ferric oxide which has been stabilized as a pure nanophase in the form of nanoparticles,[1,2] nanowires,[3−5] or nanorods.[6] Spherical particles, nanowires,[5] and nanorods were produced in silica matrices *via* sol−gel inspired methods followed by heat treatments at relatively high temperatures. In the case of nanowires[3,4] the stabilization of epsilon has been achieved on an Au−alumina substrate by pulsed laser deposition where the gold particles acted as catalyst.

It is well-known that maghemite (γ-Fe_2O_3) is a metastable polymorph that transforms to hematite (α-Fe_2O_3) around 400 °C. However, the stability of γ-Fe_2O_3 can be maintained up to 1000 °C when the particles are confined in a silica matrix. Above this temperature, and for a given range of crystallite sizes, the transformation into ε-Fe_2O_3 begins. This has been explained in terms of a lower bulk free energy and higher surface energy values of the epsilon phase as compared to maghemite.[7,8]

The crystal structure of ε-Fe_2O_3 is orthorhombic ($Pna2_1$, $a = 5.0885$ Å, $b = 8.7802$ Å, $c = 9.4709$ Å at 200 K) with Fe occupying four distinct crystallographic sites, including one tetrahedral (T_d: Fe_T) and three octahedral (O_h: one regular (Fe_{RO}) and two distorted (Fe_{DO1}), (Fe_{DO2})) (see the unit cell in the Supporting Information, Figure S1). The high temperature magnetic structure of ε-Fe_2O_3 is that of a collinear ferrimagnet with the Fe^{3+} magnetic moments antiferromagnetically coupled along *a*. The Fe^{3+} magnetic moments in the (Fe_{DO1}) and (Fe_{DO2}) distorted octahedral sites mutually cancel, and the net magnetization of this phase results from the uncompensated magnetic moments of the atoms in tetrahedral (Fe_T) and regular octahedral (Fe_{RO}) positions yielding a net magnetization of ~0.3 μ_B per Fe^{3+} at room temperature.[9] Concerning other magnetic properties, ε-Fe_2O_3 exhibits a moderate anisotropy, $K \approx 5 \times 10^6$ erg/cm^3, leading to a large coercivity (H_C) of ~20 kOe at room temperature which collapses to ~0.8 kOe at around 110 K[10,11] (see HC(T) in Supporting Information, Figure S2). In addition, its magnetic and dielectric properties are coupled.[12] The magnetic softening, accompanied by a decrease in the dielectric constant, has been related to a commensurate to incommensurate magnetic transition and the concomitant decrease of the magnetocrystalline anisotropy. Recently we have reported that the spin−lattice coupling at temperatures above 200 K is responsible for the large coercivity values and likely for the magnetoelectric behavior found in this iron oxide phase.[13]

Consequently, the interest in ε-Fe_2O_3 is owed to its rich magnetic phase diagram and magnetoelectric properties not found in other simple ferric oxides. In addition, an appealing potential application has recently been presented by the Ohkoshi's group reporting the use of ε-Fe_2O_3 as electromagnetic wave absorber in the millimeter range. They showed that the frequency of the absorption band can be tuned by Ga^{3+} or Al^{3+} substitution in the tetrahedral Fe^{3+} sites.[14,15]

*Address correspondence to roig@icmab.es.

Received for review June 26, 2009 and accepted October 7, 2009.

Published online October 13, 2009.
10.1021/nn901022s CCC: $40.75

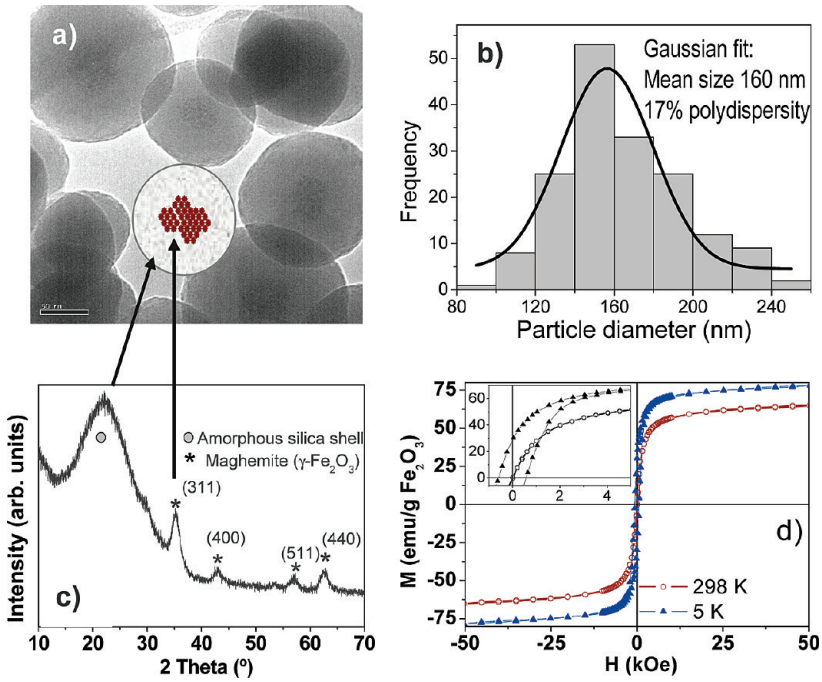

Figure 1. (a) TEM image showing a homogeneous γ-Fe_2O_3/SiO_2 composite; scale bar is 50 nm, (b) particle size histogram fitted to a Gaussian function, (c) X-ray diffractogram, (d) magnetization curves *vs* applied field, M(*H*), at room temperature and 5 K. The magnetization is referred to the mass of iron oxide. Inset: zoom at low magnetic field to show the absence and presence of a coercive field at 298 and 5 K, respectively (same units as in the nonenlarged graph).

It has been proposed that such an absorber could be used as an electromagnetic isolator in the next generation of electronic devices for high-speed wireless communications as well as to prevent unnecessary electromagnetic exposure of humans.

The potential of this material has not been fully exploited because of the difficulties encountered, initially obtaining the material as a pure phase, and lately in producing it in a suitable shape useful to be integrated in devices. The majority of systems investigated up to now have been nanocomposite powders of ε-Fe_2O_3 nano-objects in a silica matrix or aggregates of epsilon particles or nanowires without supporting matrix. The challenge is to produce ε-Fe_2O_3 in a more controlled manner and with a variety of shapes to facilitate its technological use and its integrations in devices. In that direction, some advances have already been made; ε-Fe_2O_3 nanorods could be aligned inside a silica matrix by a magnetic field.[16] In addition, nanocomposite spheres have recently been reported[17] although the shape of the reported loops reveals that ε-Fe_2O_3 only represented a minor fraction of the ferric oxide phases. Interestingly, a colloidal crystal was fabricated from an aqueous dispersion of those composite nanospheres.

Here, we report on an alternative method to fabricate ε-Fe_2O_3/SiO_2 nanospheres with a core−shell structure. The crystallization process has been optimized to obtain ε-Fe_2O_3 as the major phase and a large majority of spheres containing a single ε-Fe_2O_3 nanocrystal as a core surrounded by an amorphous SiO_2 shell. The thick silica shell has the advantage of weakening dipole−dipole interactions between composite particles avoiding aggregation due to magnetostatic attraction and thus facilitating their stability in aqueous and alcoholic solutions which in turn broadens its potential for applications such as, among others, specialty paintings for microwave shielding.

RESULTS AND DISCUSSION

The main features of the starting material, γ-Fe_2O_3/SiO_2, are displayed in Figure 1. Microscopically the starting material consists of monodisperse, nonaggregated, nanocomposite particles with a mean diameter of 160 nm and 17% polydispersity. An average of 130 maghemite nanoparticles (with mean diameter 7.5

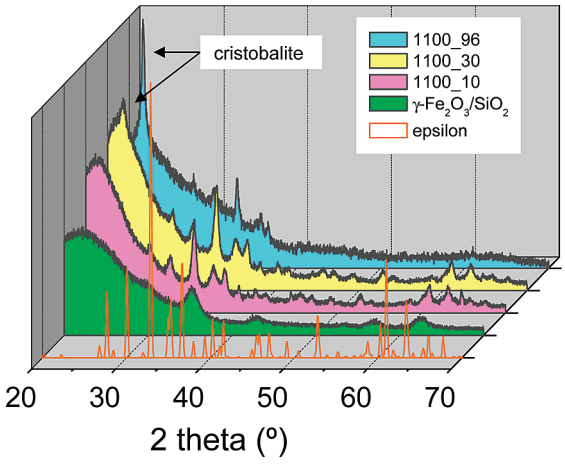

Figure 2. X-ray diffractogram of samples γ-Fe_2O_3/SiO_2, Fe_2O_3_1100_10, Fe_2O_3_1100_30, Fe_2O_3_1100_96. The pure epsilon pattern has been included for comparison.

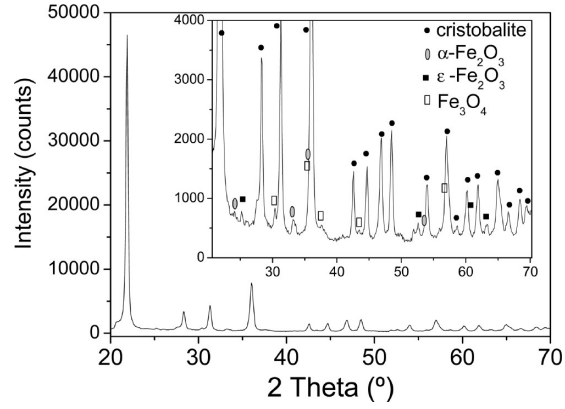

Figure 3. X-ray diffractogram of sample Fe_2O_3_1300_6h; cristobalite is the most visible phase. The inset contains a zoom at low intensities.

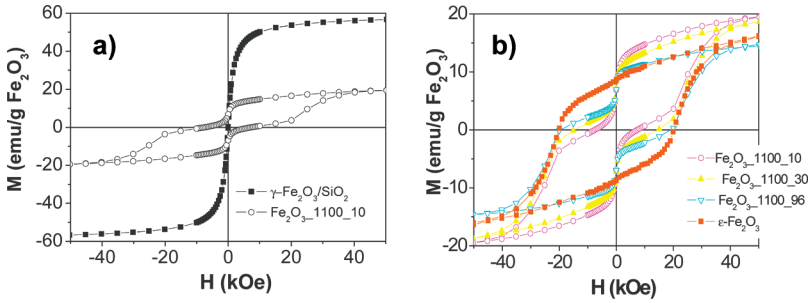

Figure 4. (a) Magnetization curves for γ-Fe_2O_3/SiO_2 and Fe_2O_3_1100_10 and (b) magnetization curves for Fe_2O_3_1100_10, Fe_2O_3_1100_30, Fe_2O_3_1100_96, and pure ε-Fe_2O_3 from *J. Appl. Phys.* 2005, *98*, 044307.

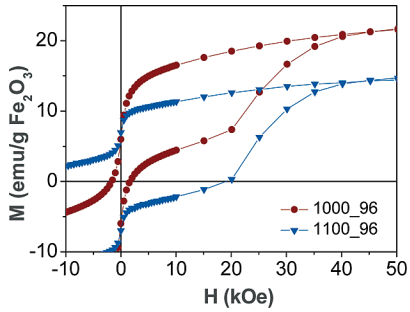

Figure 5. Magnetization curves of Fe_2O_3_1000_96 and Fe_2O_3_1100_96.

nm) are clustered in the center and surrounded by a silica shell (see Figure 1a−c). The material behaves superparamagnetically at room temperature and presents a high saturation magnetization (57 emu/g Fe_2O_3) (see Figure 1d). Recrystallization of maghemite to ε-Fe_2O_3 was achieved by annealing at different temperatures during several time lengths. Phase transition was monitored by X-ray diffraction (XRD), magnetometry, and transmission electron microscopy (TEM). The starting material is labeled as γ-Fe_2O_3/SiO_2 and the different materials obtained by thermal annealing of the former have been respectively labeled as Fe_2O_3_T _t, where T is the annealing temperature in °C and t the annealing time in hours.

Calcination of γ-Fe_2O_3/SiO_2 nanoparticles in air following a specific heating protocol consisting of 3 h of calcination every 100 °C from 300 up to 1100 °C (and increasing calcination times at 1100 °C: 6, 10, 30, 96 h) yielded ε-Fe_2O_3/SiO_2 nanoparticles. No remarkable differences in terms of size, phase, and magnetic properties could be observed between the Fe_2O_3_1100_6 and Fe_2O_3_1100_10 samples. The ε-Fe_2O_3 phase was already very prominent and the major phase after 6 h of annealing. Figure 2 shows the X-ray diffractograms of γ-Fe_2O_3/SiO_2, Fe_2O_3_1100_10, 30, and 96 h. Epsilon pattern has also been included. After 10 h of calcination, only the epsilon phase, as well as amorphous silica, can be identified from X-ray data. The main peak of cristobalite (silica crystalline phase) starts to appear in the materials annealed during 30 h and it is more visible for those annealed during 96 h.

Annealing at higher temperature, 1300 °C, produced the full crystallization of the amorphous silica into cristobalite and the transformation of ε-Fe_2O_3 into hematite, as the major iron oxide phase, and magnetite (see Figure 3).

Measurements of magnetization *vs* magnetic field for the above materials annealed at 1100 °C and of pure maghemite and ε-Fe_2O_3 are included in Figure 4. These measurements indicate that the original maghemite, which could not be identified by X-ray dif-

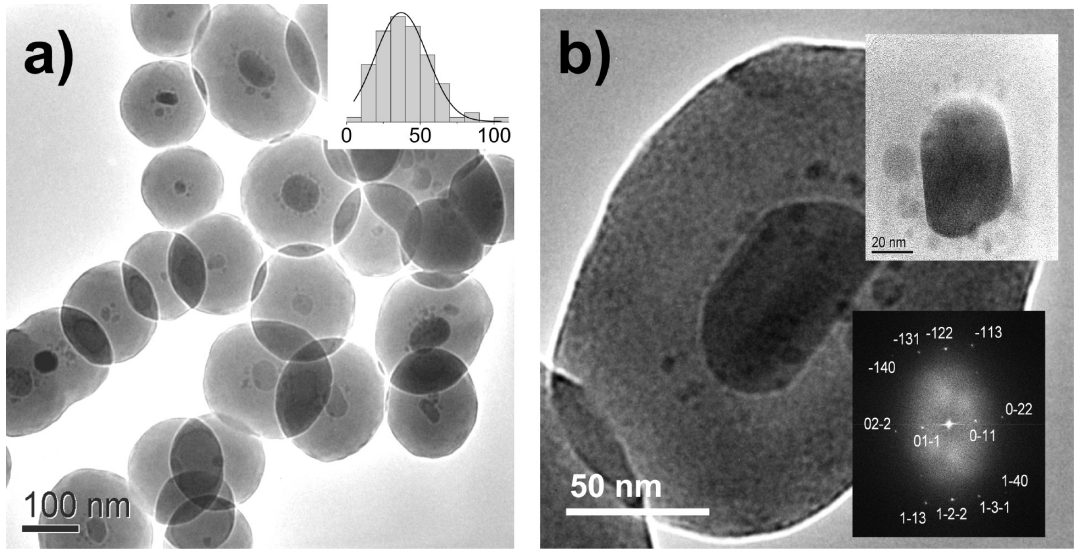

Figure 6. (a) TEM image of samples Fe_2O_3_1100_6; inset shows the epsilon particle size distribution giving a mean size of 37 nm with 50% polydispersity, and (b) TEM image zoomed in a single particle. Top inset shows an epsilon iron oxide crystallite, bottom inset shows the indexing of the crystalline planes to the [411] zone axis of the epsilon phase.

fraction, is still present in a greater or lesser extent in the annealed materials. This is evidenced by the shape of the hysteresis loops, the value of the saturation magnetization, and the value of the coercive field. Knowing that the saturation magnetization of the starting material is 57 emu/g Fe_2O_3 and the room temperature magnetization of pure ε-Fe_2O_3 at 50 kOe is 15 emu/g, we can extrapolate from its magnetization saturation that the materials annealed at 1100 °C (10 and 30 h) consist of about 90 wt % ε-Fe_2O_3 and 10 wt % maghemite. The optimized material in terms of the smaller amount of maghemite is found for the sample annealed at 1100 °C during 30 h. The $\mathbf{M}_s$ value for the sample annealed during 96 h is slightly lower than for pure epsilon pointing to small amount of hematite (less than 5%) as a consequence of the onset of crystallization of silica as seen in Figure 2.

Annealing to slightly lower temperature, 1000 °C, for long times, 96 h, produces a material with a lower relative content in ε-Fe_2O_3 as revealed by the magnetic measurements presented in Figure 5 where the magnetization curves of Fe_2O_3_1000_96 and Fe_2O_3_1100_96 are displayed.

Morphology changes and phase transformation could be monitored by TEM. The original material, γ-Fe_2O_3/SiO_2, is formed by a nanoparticle composite with many iron oxide nanoparticles clustered in the center of the silica nanosphere (see Figure 1a). In the material obtained after calcination at 1100 °C for 6 h, Fe_2O_3_1100_6, the composite particle shape does not change and the particles are very monodisperse with no appreciable degree of necking. The relevant feature at this stage is that the clustered iron oxide nanoparticles have sintered forming a single ε-Fe_2O_3 nanocrystal (of diameters ranging from 20 to 100 nm) also placed at the center of the silica shell (see Figure 6a). Zooming at the center of one composite particle an ε-Fe_2O_3 single crystal can be indentified. The crystalline planes could be indexed to the [411] zone axis of the epsilon phase (see Figure 6b). Figure 6 panels a and b show the "satellites" of what we assume are maghemite nanoparticles around the central epsilon particle.

Calcination at 1100 °C for 30 h causes the silica shells to begin sintering and, even though the spherical shape is well maintained, some necking between the particles starts to appear (see Figure S3a in Supporting Information); this is more pronounced for the sample annealed at 96 h. Finally, when the particles are annealed up to 1300 °C and the silica has crystallized to cristobalite the material presents irregular shape as seen in Figure S3b in Supporting Information.

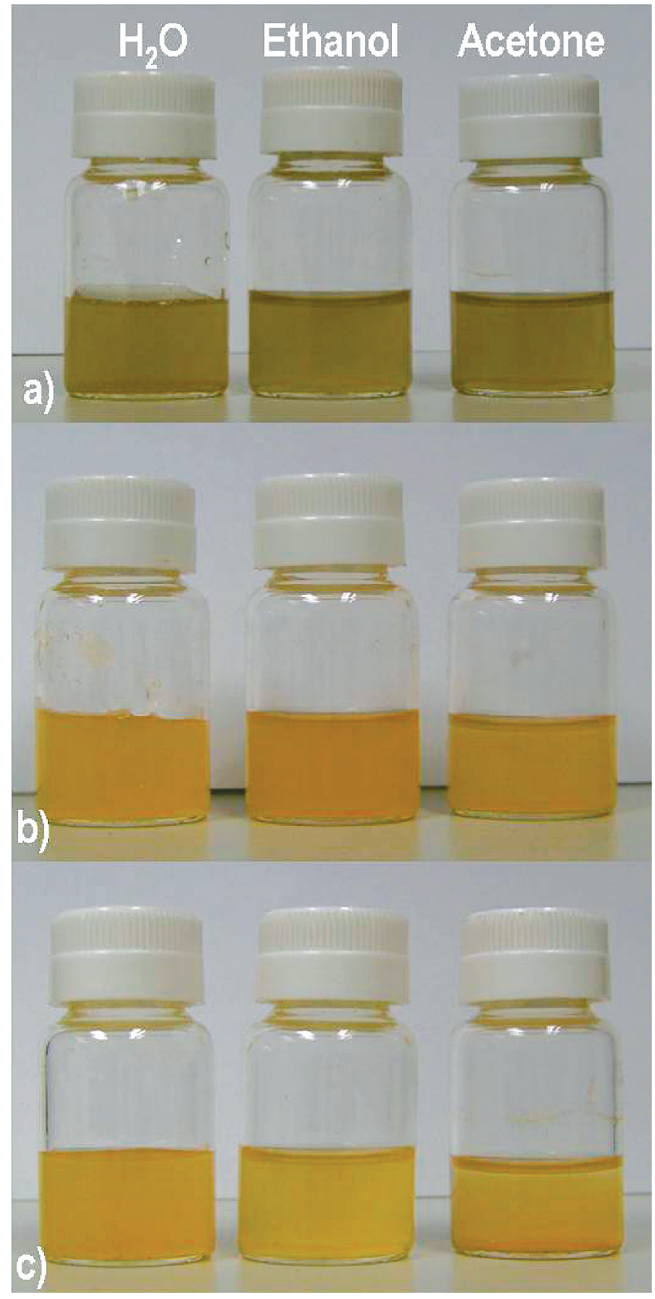

Figure 7. Pictures displaying colloidal dispersions in water, ethanol, and acetone for the (a) γ-Fe_2O_3/SiO_2, (b) Fe_2O_3_1100_6, and (c) Fe_2O_3_1100_30 samples for a concentration of 0.5 mg/mL.

The composite particles could be easily dispersed as colloids in several polar solvents (water, ethanol, and acetone), and they were undispersible in hexane. Figure 7 displays the dispersions for the γ-Fe_2O_3/SiO_2, Fe_2O_3_1100_6, and Fe_2O_3_1100_30 samples (0.5 mg/mL). Such dispersions are stable for around 12 h although they get easily redispersed by a short sonification (same behavior was observed for concentrations of 1 mg/mL). Note the difference in color of the γ-Fe_2O_3/SiO_2 dispersion (ochre) compared to the Fe_2O_3_1100_6/30 ones (orange). Color can be used as a fast visual

test to monitor the phase transformation. Colloidal suspensions of materials calcined for shorter time periods (6−10 h) are more stable than the ones treated for longer times (30−96 h). In the later case, necking formation within the particles produces larger aggregates and induces faster sedimentation. Dynamic light scattering (DLS) measurements were also performed, the results are displayed in Figure S4 in Supporting Information. The calculated hydrodynamic size is defined as the diameter not only of the particle, but also of the solvent molecules strongly adsorbed onto its surface. Therefore, the hydrodynamic size is always larger than the size observed by TEM. Furthermore, the scattering intensity depends on the sixth power of the particle radius meaning that larger particles contribute more to the average size than the smaller ones. In our case the DLS size is about double the one determined by TEM. As it applies to both the as-obtained materials and the calcined ones, we ascribe it to the formation of dimers; such a result does not prevent the colloidal stability of the system.

As mentioned in the introduction and confirmed by this work, the stability of γ-Fe_2O_3 nanoparticles can be maintained up to 1000 °C when the particles are confined in a silica matrix. Above this temperature, and for a given range of crystallite sizes, the transformation into ε-Fe_2O_3 starts. This has been explained in terms of a lower bulk free energy and higher surface energy values of the epsilon phase as compared to that of maghemite.[7,8] Our nanocomposite particles follow this same pattern. The silica coating limits the particle growth and enables the formation of epsilon iron oxide single crystals except for the outermost maghemite crystals unable to migrate close enough to the large epsilon crystal. At 1300 °C the amorphous silica shell crystallizes to cristobalite, and the iron oxide phase segregates and grows further, forming hematite and magnetite.

CONCLUSIONS

The present study provides a route to synthesize single crystals of ε-Fe_2O_3 individually wrapped in a silica shell; the material was obtained by controlled recrystallization of a group of maghemite particles confined in a microporous silica nanosphere. The formation of ε-Fe_2O_3/silica core−shell particles and the tuning of the magnetic properties are possible *via* calcination in air of maghemite/silica composite particles at 1100 °C from 6 to 96 h. The epsilon particle size could be controlled by selecting starting materials of maghemite/silica composite particles with different magnetic cluster size as reported in Taboada *et al.*[19] The composite nanoparticles prepared in this work can be dispersed to form a colloidal suspension in several polar liquids, enlarging in this way the processability of the material and making feasible the controlled deposition of epsilon single crystals onto surfaces. In particular, potential applications of this material as specialty paintings for microwave shielding could be envisaged.

METHODS

Synthesis. A detailed account on the synthetic procedure to prepare the maghemite particles confined in silica shells which were used as starting material is reported in Taboada *et al.*[18,19] Briefly, maghemite nanoparticles (γ-Fe_2O_3) were synthesized by a modification of the method developed by Hyeon *et al.*[20] showing a mean diameter of 7.5 nm, narrow particle size distribution (<10% polydispersity), and superparamagnetic behavior at room temperature. The silica coating of the maghemite nanoparticles was done in a one-pot approach, combining sol−gel hydrolysis and condensation of a silicon precursor and supercritical evacuation of the solvent. Initial reagents with a volume composition (mL) TMOS/H_2O/acetone/Fe_2O_3_hexane = 3.72/190/0.9/10 (and V_{acet}/V_{hex} = 150) were placed in a Pyrex vessel at ambient conditions; the vessel was then placed inside an autoclave, and the pressure was increased to 50 bar. Afterward, temperature was raised up to 250 °C with the corresponding increase of pressure to 250 bar. The final P and T values were over the critical point of the CO_2/acetone mixture (P_c (max) = 120 bar and T_c (max) = 235 °C). After 2 h of reaction at supercritical conditions the autoclave was depressurized up to 150 bar and fresh CO_2 was circulated. The resulting material is a dry, light powder homogeneously distributed on the reactor walls. It behaves as a superparamagnet at room temperature and presents a high saturation magnetization (57 emu/g Fe_2O_3) (see Figure 1c).

Chemical Analysis. Elemental composition was measured by inductively coupled plasma mass spectroscopy (ICP−MS). Starting material was digested with a mixture of HNO_3 and HF in a microwave oven. Digestion of control samples was also performed and analyzed resulting in 6.5 wt % of Fe_2O_3.

XRD. The composite samples were characterized by X-ray diffraction with a Siemens D5000 and a Rigaku Rotaflex RU-200 B, both with copper Kα incident radiation (λ = 1.54 Å).

Magnetic Measurements. Magnetization *vs* applied magnetic field was measured with a superconducting quantum interference device (SQUID) magnetometer (Quantum Design MPMS5XL). All the magnetization data are presented in units of emu/g iron oxide (equivalent to Am^2/kg iron oxide).

TEM. A JEOL JEM-1400 operating at 200 keV was used for the microstructure analysis. To observe the materials, a drop of diluted acetone dispersion was deposited onto a TEM carbon grid and allowed to dry. Aqueous dispersions were avoided to prevent the formation of silica necking at the contact area between particles when exposed to the high energy beam.

DLS. A Zetasizer Nano ZS from Malvern Instruments, equipped with a He/Ne 633 nm laser was used. DLS measures Brownian motion and relates it to the size of the particles. It does this by illuminating the particles with a 633 nm laser and analyzing the intensity fluctuations in the scattered light at 173°. Every sample was measured three times and every measurement is in turn composed of 10−20 runs, depending on the solvent and concentration. An average value is obtained for each sample.

Acknowledgment. This work has been partially funded by the Ministerio de Ciencia e Innovacion (MAT2009-08024 and CONSOLIDER-NANOSELECT-CSD2007-00041) and the Generalitat de Catalunya (2009SGR203). Fundación Domingo Martínez is also kindly acknowledged.

Supporting Information Available: ε-Fe_2O_3 unit cell; temperature dependence of several magnetic parameters in ε-Fe_2O_3; TEM images of Fe_2O_3_1100_30 and Fe_2O_3_1300_10; DLS size dis-

tribution by number of γ-Fe_2O_3/SiO_2, Fe_2O_3_1100_6, and Fe_2O_3_1100_30 in several polar solvents. This information is available free of charge *via* the Internet at http://pubs.acs.org.

REFERENCES AND NOTES

1. Jin, J.; Ohkoshi, S.; Hashimoto, K. Giant Coercive Field of Nanometer-Size Iron Oxide. *Adv. Mater.* **2004**, *16*, 48–51.
2. Popovici, M.; Gich, M.; Nižňanský, D.; Roig, A.; Savii, C.; Casas, Ll.; Molins, E.; Zaveta, K.; Enache, C.; Sort, J.; de Brion, S.; Chouteau, G.; J. Nogués, J. Optimized Synthesis of the Elusive ε-Fe_2O_3 Phase *via* Sol−Gel Chemistry. *Chem. Mater.* **2004**, *16*, 5542–5548.
3. Ding, Y.; Morber, J. R.; Snyder, R. L.; Wang, Z. L. Nanowire Structural Evolution from Fe_3O_4 to ε-Fe_2O_3. *Adv. Funct. Mater.* **2007**, *17*, 1172–1178.
4. Morber, J. R.; Ding, Y.; Haluska, M.; Li, Y.; Liu, J. P.; Wang, Z. L.; Snyder, R. L. PLD-Assisted VLS Growth of Aligned Ferrites Nanorods, Nanowires, and Nanobelts−Synthesis and Properties. *J. Phys. Chem. B* **2006**, *110*, 21672–21679.
5. Sakurai, S.; Tomita, K.; Hashimoto, K.; Yashiro, H.; Okhosi, S. Preparation of the Nanowire Form of Epsilon-Fe_2O_3 Single Crystal and a Study of the Formation Process. *J. Phys. Chem. C* **2008**, *112*, 20212–20216.
6. Jin, J.; Hashimoto, K.; Ohkoshi, S. Formation of Spherical and Rod-Shaped ε-Fe_2O_3 Nanocrystals with Large Coercive Field. *J. Mater. Chem.* **2005**, *15*, 1067–1071.
7. Gich, M.; Roig, A.; Taboada, E.; Molins, E.; Bonafos, C.; Snoeck, E. Stabilization of Metastable Phases in Spatially Restricted Fields. The Case of Fe_2O_3 Polymorphs. *Faraday Discuss.* **2007**, *136*, 345–354.
8. Ohkoshi, S.; Sakurai, S.; Jin, J.; Hashimoto, K. The Additions Effects of Alkaline Earth Ions in the Chemical Synthesis of ε-Fe_2O_3 Nanocrystals that Exhibit a Huge Coercive Fields. *J. Appl. Phys.* **2005**, *97*, 10K312-1–10K312-3.
9. Tronc, E.; Chanéac, C.; Jolivet, J. P. Spin Collinearity and Thermal Disorder in ε-Fe_2O_3. *J. Solid State Chem.* **1998**, *139*, 93–104.
10. Gich, M.; Roig, A.; Frontera, C.; Molins, E.; Sort, J.; Popovici, M.; Chouteau, G.; D. Martín, Y.; Marero, D.; Nogués, J. Large Coercivity and Low Temperature Magnetic Reorientation in ε-Fe2O3 Nanoparticles. *J. Appl. Phys.* **2005**, *98*, 044307-1–044307-5.
11. Gich, M.; Frontera, C.; Roig, A.; Taboada, E.; Molins, E.; Rechenberg, H. R.; Ardisson, J. D.; Macedo, W. A. A.; Ritter, C.; Hardy, V.; *et al*. High and Low-Temperature Crystal and Magnetic Structures of ε-Fe_2O_3 and Their Correlation to Its Magnetic Properties. *Chem. Mater.* **2006**, *18*, 3889–3897.
12. Gich, M.; Frontera, C.; Roig, A.; Fontcuberta, J.; Molins, E.; Bellido, N.; Simon, Ch.; Fleta, C. Magnetoelectric Coupling in ε-Fe_2O_3 Nanoparticles. *Nanotechnology* **2006**, *17*, 687–691.
13. Tseng, Y. C.; Souza-Neto, N. M.; Haskel, D.; Gich, M.; Frontera, C.; Roig, A.; van Veenendaal, M.; Nogués, J. Nonzero Orbital Moment in High Coercivity ε-Fe_2O_3 and Low-Temperature Collapse of the Magnetocrystalline Anisotropy. *Phys. Rev. B* **2009**, *79*, 094404_1–094404_6.
14. Namai, A.; Sakurai, S.; Nakajima, M.; Suemoto, T.; Matsumoto, K.; Goto, M.; Sasaki, S.; Ohkoshi, S. Synthesis of an Electromagnetic Wave Absorber for High-Speed Wireless Communications. *J. Am. Chem. Soc.* **2009**, *131*, 1170–1173.
15. Ohkoshi, S.; Kuroki, S.; Sakurai, S.; Matsumoto, K.; Sato, K.; Sasaki, S. A Millimeter-Wave Absorber Based on Gallium-Substituted ε-Iron Oxide Nanomagnets. *Angew. Chem., Int. Ed.* **2007**, *46*, 8392–8395.
16. Sakurai, S.; Shimoyama, J.; Hashimoto, K.; Ohkoshi, S. Large Coercive Field in Magnetic-Field Oriented ε-Fe_2O_3 Nanorods. *Chem. Phys. Lett.* **2008**, *458*, 333–336.
17. Nakamura, T.; Yamada, Y.; Yano, K. Novel Synthesis of Highly Monodispersed γ-Fe_2O_3/SiO_2 and ε-Fe_2O_3/SiO_2 Nanocomposite Spheres. *J. Mater. Chem.* **2006**, *16*, 2417–2419.
18. Taboada, E.; Rodriguez, E.; Roig, A.; Oro, J.; Roch, A.; Muller, R. N. Relaxometric and Magnetic Characterization of Ultrasmall Iron Oxide Nanoparticles with High Magnetization. Evaluation as Potential T_1 Magnetic Resonance Imaging Contrast Agents for Molecular Imaging. *Langmuir* **2007**, *23*, 4583–4588.
19. Taboada, E.; Solanas, R.; Rodríguez, E.; Weissleder, R.; Roig, A. Supercritical Fluid Assisted One-Pot Synthesis of Biocompatible Core(γ-Fe_2O_3)@Shell(SiO_2) Nanoparticles as High Relaxivity T_2-Contrast Agents for Magnetic Resonance Imaging. *Adv. Funct. Mater.* **2009**, *19*, 2319–2324.
20. Hyeon, T.; Lee, S. S.; Park, J.; Chung, Y.; Bin, N. H. Synthesis of Highly-Crystalline and Monodisperse Maghemite Nanocrystallites without a Size-Selection Process. *J. Am. Chem. Soc.* **2001**, *123*, 12798–12801.